Effect of mean shear stress on the fatigue strength of notched components under multiaxial stress state

Mohamed Bennebach, Thierry Palin-Luc, Alexandre Messager

Available online at www.sciencedirect.com

ScienceDirect

Procedia Engineering 213 (2018) 25–35

Procedia Engineering

www.elsevier.com/locate/procedia

7th International Conference on Fatigue Design, Fatigue Design 2017, 29-30 November 2017, Senlis, France

Effect of mean shear stress on the fatigue strength of notched components under multiaxial stress state.

M. Bennebach[a*], T. Palin-Luc[b], A. Messager[b]

[a]CETIM, 52 avenue Felix Louat, 60304 Senlis cedex, France
[b]Arts et Metiers ParisTech, I2M Bordeaux, CNRS, Esplanade des Arts et Metiers, 33405 Talences cedex, France

Abstract

The effect of a static and intermittent shear stress on the HCF strength of two quenched and tempered steel grades used to produce shafts in crane industry was studied on notched specimens ($K_{t,bending}$=1.7 and 2.7) for being representative of critical areas. Three main loading configurations were considered: C1=rotative bending (RB), C2=RB and static torsion and C3=RB and mean torsion fluctuating in blocks to simulated start and stop cycles. In this last case the first investigated mean shear stress, τ_m, was equal to the material yield stress in pure shear, τ_y. Additional C3 variants were investigated too where τ_m was equal to $0.3\tau_y$ and $0.7\tau_y$. It has been shown that τ_m has little effect on the rotating bending HCF strength at 3×10^6 cycles. For both steel grades and notch geometries studied, the results of the fatigue tests confirm that the influence of a static torsion on the rotating bending HCF strength is negligible even when the static torsion level is equivalent to the yield strength of the material in torsion. However, in intermittent service conditions (C3), it has been shown that torsion cycles can affect significantly the HCF strength in RB, depending on the notch acuity and torsion level. Elastic-plastic cyclic finite element analysis has been done for the two specimen geometries to assess the stabilized stress-strain state at the notch root and then compute the fatigue life by using the multiaxial HCF models proposed by: Fatemi-Socie, Smith-Watson-Topper, and Wang-Brown. The Palmgreen-Miner hypothesis was used to cumulate damage mainly because of its simplicity for design purposes. According to our simulations and with the chosen cumulative damage rule, none of the tested fatigue life calculation methods give good results for all the load cases. The efficiency of the tested methods is very dependent on both the material and the load cases. However, the Smith-Watson-Topper approach gives the best results whereas the Fatemi-Socie model leads to the more conservative ones except in one load configuration.

Peer-review under responsibility of the scientific committee of the 7th International Conference on Fatigue Design.

Keywords: Multiaxial loadings; Notched components, Variable amplitude; Mean shear stress; Fatigue life; Combined bending and torsion

1. Introduction

For some sectors such as cranes or power transmission industries, shafts design is mainly based on specific methods developed in national or international standards [1,2]. These methods rely on very simple approaches that may not correctly cover the large range of materials and loadings involved. To remedy possible inaccuracies due to numerous simplifications, these methods use a set of correction factors in the calculation of safety factors that are usually too pessimistic. This leads in general to over conservative life assessments and non-optimized designs.

One possible explanation of this over conservatism is the usage made by these methods of the mean shear stress. The latter is by default included in the calculation of an equivalent fatigue stress though in high cycle multiaxial fatigue it is usually admitted that mean shear stress has no significant effect on the fatigue strength, even for values of the maximum shear stress that may approach the material shear yield limit.

Peer-review under responsibility of the scientific committee of the 7th International Conference on Fatigue Design.
10.1016/j.proeng.2018.02.004

Most of the experimental results available in the bibliography being on un-notched (smooth) specimens, CETIM and ENSAM have carried out a consistent fatigue test campaign in order to investigate the effect of a static and intermittent shear stress on two quenched and tempered steels used for shaft fabrication. In a first part, this paper summarizes the experimental procedure and results obtained. Then, a second part aims to use numerical simulation to evaluate the stress and strain state at the notch root and compare predictions of several high cycle multiaxial fatigue criteria with experimental results.

2. Experimental program and test results

2.1. Materials and specimens

The materials used for the experimental campaign are two quenched and tempered (QT) steel grades, 30NiCrMo8 and 42CrMo4. These grades are often used for machinery shafts requiring high resistance. Tables 1 to 3 give their chemical compositions and mechanical properties under monotonic quasi-static tension.

Table 1. Chemical composition of the 30NiCrMo8 steel.

Element	C	Mn	Si	P	S	Cr	Ni	Mo	Cu	Al	Sn	Ca
[w%]	0.290	0.530	0.310	0.011	0.026	2.050	1.950	0.350	0.190	0.028	0.014	0.0008

Table 2. Chemical composition of the 42CrMo4 steel.

Element	C	Mn	Si	P	S	Cr	Ni	Mo	Cu	Al
[w%]	0.400	0.870	0.350	0.015	0.022	1.020	0.220	0.164	0.190	0.022

Table 3. Mechanical properties under monotonic quasi-static tension of the QT steels

Steel grade	30NiCrMo8	42CrMo4
Tensile strength, R_m (MPa)	1104	1061
Tensile yield strength, $R_{p0.2}$ (MPa)	995	990
Elongation at failure, A%	13.9	14.6

Since in a part of this study it is important to check the influence of a static torsion in the presence of stress concentrations representative of real components, cylindrical specimens with circular notches are considered. This allows carrying out tests with conventional fatigue testing machines on specimens having a simple geometry. The theoretical stress concentration factors of 2.7 (0.5 mm notch radius) and 1.7 (1.8 mm notch radius) in bending were selected. These K_t are consistent with the values generally observed, which are between 1.5 and 3. Figure 1 illustrates the specimens' geometry.

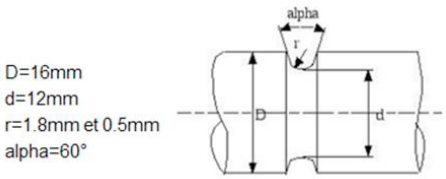

Fig. 1: Notched geometries tested

2.2. Multiaxial fatigue testing equipment

All tests were performed on the same test bench at I2M Bordeaux (ENSAM, Bordeaux campus) on a servo-hydraulic multi-actuators fatigue testing machine for applying combined loadings of bending and torsion. The machine's mechanical principal and capabilities are described in details in [3].

2.3. Testing procedure

The fatigue tests were performed for both materials and geometries selected, according to the stair-case method, with different load configurations, namely: rotating bending only (C1); rotating bending + static torsion (C2); rotating bending + static torsion with an intermittent regime (simulating starts and stops of a machine), named C3. For each load configuration, the fatigue strengths at 3×10^6 cycles (named endurance limit in the following) under rotating bending were determined.

For tests in intermittent operation (load case C3), the number of starts-stops chosen in consultation with the relevant industry led to about 2000 repeated torsion cycles on 3×10^6 maximum total cycles for the test. For the stress levels applied in static torsion, the tests were carried out with 100%, 70% and 30% of the yield strength in torsion of the tested QT steels. For both materials, this yield strength is about 575 MPa. The high level at 100% is chosen voluntarily according to the bibliographic knowledge in order to highlight a possible influence of the mean torsion on the HCF strength of the steels. All the tests were performed at room temperature, in air and at a frequency of 50 Hz. About 150 specimens were tested in total. The tests were stopped when the specimen stiffness decreased of 20% corresponding to a macroscopic crack.

2.4. Test results and discussion

Results on 30NiCrMo8

Table 4 summarizes the results on the 30NiCrMo8 steel grade for the different loading conditions. Values reported are the median endurance limits (survival probability of 50%) in rotating bending at 3×10^6 cycles and associated standard deviation (s). The stress values are the local elastic ones, including the effect of the theoretical stress concentration factor, Kt.

Whatever K_t, the influence of a static torsion on the rotating bending fatigue strength results in only a slight decrease (< 8%), not really significant especially if one takes into account the experimental scatter. The addition of an intermittent torsion, simulating starts-stops can significantly affect the endurance limit in rotating bending in the case of $K_t = 2.7$, depending on the torsion stress level applied. A maximum torsion level equal to the yield strength in torsion reduces the endurance limit in rotating bending by nearly 30%. This reduction is of 20% for a level corresponding to 70% of the yield strength and almost zero for 30% of the yield strength. Under intermittent regime (C3) no effect was observed for $K_t = 1.7$.

Table 4. Results on 30NiCrMo8 (s = standard deviation)

	Rotating bending endurance limit (MPa, local elastic value)	
Loading	$K_t = 2,7$	$K_t = 1,7$
Rotating bending only (C1)	580 (s=60)	550 (s=13)
Rotating bending + static torsion (C2) (τ_m = 100% of yield strength in torsion)	537 (s=55)	545 (s=10)
Rotating bending + static torsion, intermittent regime (C3, 100%) (τ_m = 100% of yield strength in torsion)	401 (s=20)	540 (s=33)
Rotating bending + static torsion, intermittent regime (C3, 70%) (τ_m = 70% of yield strength in torsion)	470 (s=33)	-
Rotating bending + static torsion, intermittent regime (C3, 30%) (τ_m = 30% of yield strength in torsion)	570 (s=20)	-

Results on 42CrMo4

For this steel grade, the tests have been conducted with four loading conditions only on $K_t = 2.7$. Table 5 gives the results obtained in terms of rotating bending endurance limits and associated scatter.

Table 5. Results on 42CrMo4 (s = standard deviation)

	Rotating bending endurance limit (MPa, local elastic value)
Loading	K_t = 2,7
Rotating bending only (C1)	627 (s=40)
Rotating bending + static torsion (C2) (τ_m = 100% of yield strength in torsion)	573 (s=40)
Rotating bending + static torsion, intermittent regime (C3, 100%) (τ_m = 100% of yield strength in torsion)	430 (s=20)
Rotating bending + static torsion, intermittent regime (C3, 30%) (τ_m = 30% of yield strength in torsion)	563 (s=20)

As in the case of 30CrNiMo8, the effect of a static torsion results in only a small decrease of the endurance limit in rotating bending (< 9%). But the addition of repeated torsion cycles, simulating starts-stops leads to a 31% reduction of the rotating bending endurance limit for a static torsion level of 100% of the yield strength in torsion. This reduction is about 10% for a level of 30% of the yield strength in torsion.

General conclusions on the test results

For both steel grades and notch geometries studied in this work, the results of the fatigue tests tend to confirm that the influence of a static torsion on the median value of the rotating bending strength at 3×10^6 cycles is negligible even when the static torsion level is equivalent to the yield strength in torsion. This observation supports the HCF criteria and methods that state the independence of the HCF strength upon a superimposed mean shear stress under constant amplitude cyclic loading.

However, in intermittent service conditions where repeated cycles of torsion are introduced, it has been shown that these cycles can affect significantly the rotating bending endurance limit at 3×10^6 cycles, depending on both the notch acuity and the applied torsion level. In the case of K_t = 2.7, for both materials, the rotating bending strength reduction reached 30% for a torsion level equal to the yield strength in shear. This reduction becomes significant only for a torsion level over 30% of the yield strength in torsion. Although this effect was not observed in the case of K_t = 1.7, it seems relevant to consider in general that the damage induced by these repeated cycles is not negligible beyond a torsion level of 30% of the yield strength in shear.

These observations are complemented by the following part of this paper, where finite element simulations are carried out in order to evaluate the local stress-strain states, try to explain the observed behavior and compare life predictions given by some high cycle multiaxial fatigue criteria.

3. Finite element analysis

The FEA and the identification of the parameters of the constitutive model were carried out with the ZeBuLoN software.

3.1. Constitutive model of the two materials

The studied steels are supposed to follow the Von Mises yield criterion. The yield function is given by:

$$f(\sigma, X) = \sigma_{eq}(\sigma - X_i) - R(p) \quad (1)$$

Two isotropic hardening models were used to simulate the material behavior:

- Constant isotropic hardening: R(p) = R_0 with R_0 a material parameter to identify

– Non-linear isotropic hardening: $R(p) = R_0 + K\,(e_0 + p)^n$ where R_0, K, e_0 and n are material parameters to identify.

The evolution of the X_i variables is described thanks to the Armstrong-Frederick model [4]:

$$X_i = \frac{2}{3} C_i \alpha_i et \dot{\alpha}_\iota = \dot{\lambda}\left(n - \frac{3D_i}{2C_i} X_i\right) \quad (2)$$

where C_i and D_i constants are material parameters to be identified with LCF tests and $\dot{x} = dx/dt$.

A literature review allowed us to identify material parameters for both 42CrMo4 [5] and 30NiCrMo8 [6] QT steels. The cyclic behavior of the 42CrMo4 material has been modeled by means of a constant isotropic hardening and a non-linear kinematic hardening. The cyclic behavior of the 30NiCrMo8 material has been modeled thanks to a nonlinear isotropic hardening combined with two non-linear kinematic hardenings. In the aim of validating these elastic-plastic cyclic material models, simulation results were compared to experimental data from [6]. For both 42CrMo4 and 30NiCrMo8, models of the material behaviors were validated in a ±2% strain range.

3.2. Specimen geometry and boundary conditions

The specimen geometries are the same than those used by Bennebach [7]. The boundary conditions are similar to those proposed by Banvillet in his PhD thesis [8]. The simulations have been divided in 3 steps. During the first one, the intensity of the two forces generating the bending moment are increased with the constant direction OA (preloading under plane bending). Then, in order to simulate the rotative bending, the direction of these forces is put in rotation around the specimen longitudinal axis throughout the cyclic loading. Later, loadings are decreased with a constant direction in the last part (unloading under plane bending).

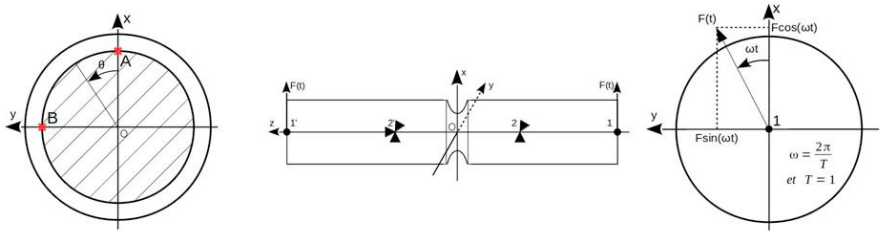

Fig. 2: Boundary conditions

4. Results of the finite element analysis

For the simulation of each load case, the number of simulated cycles was determined for having a quasi-stabilized simulated stress-strain state. Furthermore, we ensured that the maximum Von Mises equivalent strain belongs to the validity domain of the identified constitutive models (± 2% strain range).

4.1. C1 Load case: rotative bending only

4.1.1. 42CrMo4

Despite the fact that the simulated load case corresponds to the fatigue strength at $3x10^6$ cycles (HCF regime) the stabilized stress strain state of the material is not elastic shakedown but plastic one. Consequently, the cumulated plastic strain increases at each cycle. A non-intuitive result is the phase shift between the time evolution of the cumulative plastic strain at points A and B. Indeed, usually the rotative bending load is assumed to create an axisymmetric stress strain field. In fact, both the preloading and unloading steps creates a dissymmetry because local plasticity occurs during preloading and point A is loaded one more time than point B at the end just before

preloading (cumulated plastic strain is around 0.1% higher in A than in B). This phenomenon has no significant effect on the stabilized stress strain state, but the field of residual stresses is not uniform all around the notch as illustrated in Figure 3.

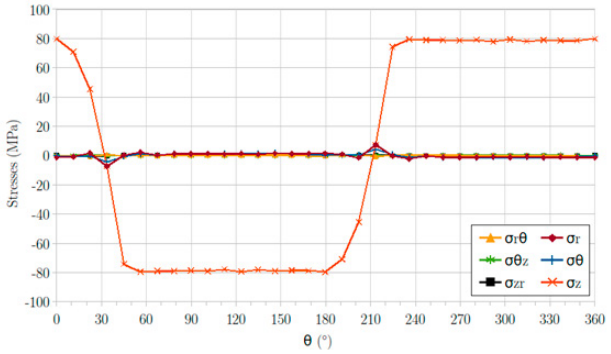

Fig. 3: Components of the residual stress tensor at the notch root all around the specimen in a cyclindral coordinate system, z is the specimen longitudinal axis.

4.1.2. 30NiCrMo8

Contrarily to the previous material and despite the high theoretical stress concentration factor (K_t=2.7 in bending) the FEA shows that the material is not plasticized at the notch root under the C1 load case. But as known in literature the stress state is not uniaxial at the notch root, ($\sigma_{\theta\theta}$= 176 MPa and σ_z = 625 MPa at the maximum of a load cycle). The maximum value of the Von Mises equivalent stress (558 MPa) is lower that the material yield strength R_0 = 565 MPa.

4.2. C2 load case: rotative bending and static torsion

4.2.1. 42CrMo4

In this case, during the preloading step, point A supports stresses due to both bending and torsion. This leads to a significant hardening of the material. But at B point (on the neutral fiber of the specimen with regard to bending) the material supports the shear stress due to torsion only. Cyclic hardening in A is greater than in B and the stabilized stress strain loops are shifted (Figure 4).

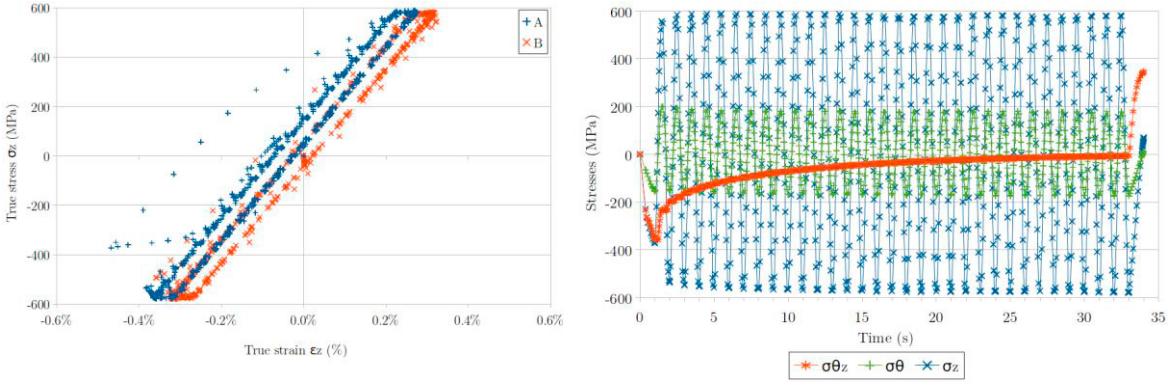

Fig. 4: C2 load case, a) stress strain loops in A and B; b) time evolution of the stresses at A on 42CrMo4 specimen

Because of the cyclic hardening of the material, the mean shear stress goes to zero. A small dissymmetry of the bending normal stress σ_{zz} can be seen ($|\sigma_{z\,Max}| \neq |\sigma_{z\,Min}|$) but this decreases with the mean shear stress relaxation.

4.2.2. 30NiCrMo8

Contrarily to the 42CrMo4 steel, the stabilized stress-strain state at the notch root of specimen in 30NiCrMo8 is elastic shakedown (Figure 5 a)) and the static shear stress is decreasing but not to zero (≈ 255MPa). For the same load case C2 on 42CrMo4, there is a mean stress in A but no mean stress and strain in B. Furthermore, there is a dissymmetry of the normal stress σ_{zz} ($\sigma_{zz,Max}$ = 602 MPa and $\sigma_{zz,Min}$ = -551 MPa) leading to a local stress ratio R ≈ -0,9).

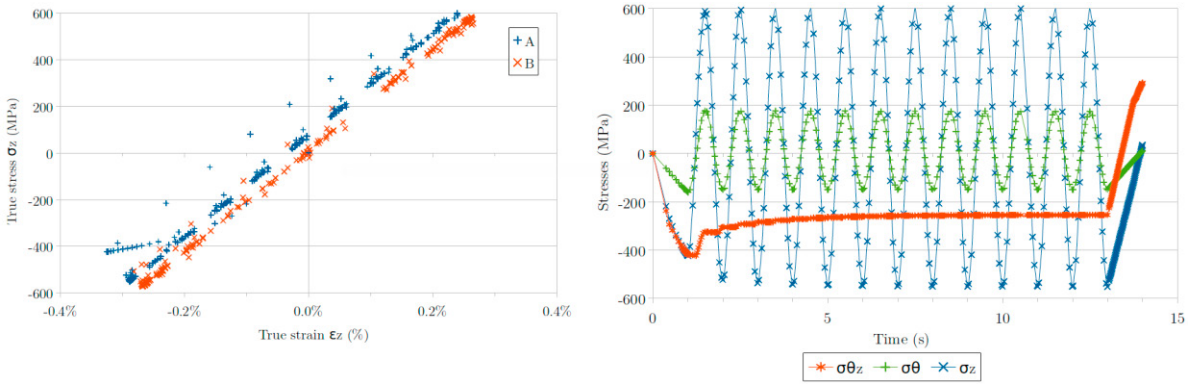

Fig. 5: C2 load case, a) stress strain loops in A and B; b) time evolution of the stresses at A on 30NiCrMo8 specimen

4.3. C3 load case: rotative bending and intermittent torsion

For the two steels of this study, it has been shown that torsion cycling appears between blocks of type 1 (with mean shear stress due to static torsion) and blocks of type 2 (without any mean torsion but with residual stresses due to plasticity). The mean shear stress is not zero at the beginning and then decreases to zero with the block alternate. For the simulations of load case C3, the normal stress evolution versus time due to rotative bending is not fully reversed (σ_{min} ≈ -380 MPa and σ_{max} ≈ 475 MPa) because of the presence of non-zero mean shear stress.

As long as the mean shear stress is not relaxed and stabilized, at each block alternate plastic strain appears and then the cumulated plastic strain increases. Then there is an elastic shakedown of the material at the notch. During the numerical simulations 4 cycles were simulated only per block to obtain stabilized stress strain loops. In reality, these cycles are numerous. Coupled with rotative bending they lead to cyclic hardening of the material.

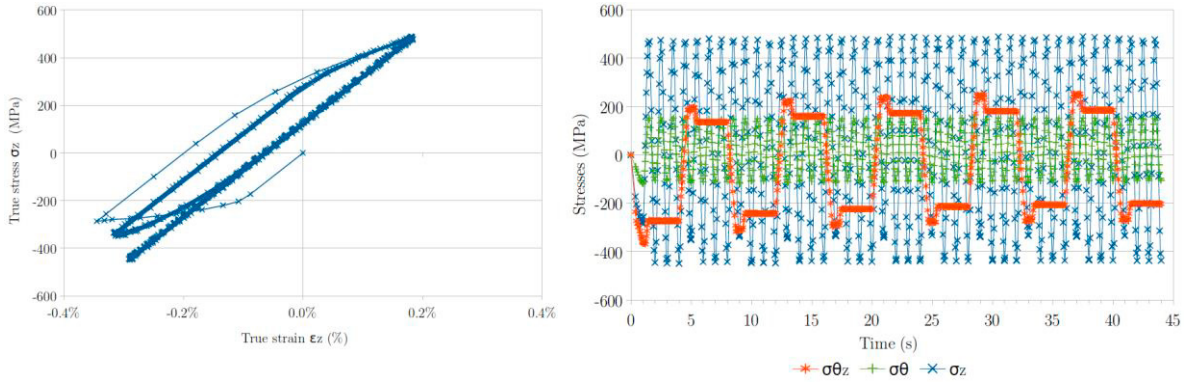

Fig. 6: C3 load case, a) stress strain loops in A; b) time evolution of the stresses at A on 42CrMo4 specimen

4.3.1. Ratcheting effect on 42CrMo4

Ratcheting has been observed on the FEA results for the 42CrMo4. In Figure 7 the blue block is one of the first and the red is one of the last of the simulated. This leads to the increase of the mean value of the longitudinal strain ε_{zz} at point B.

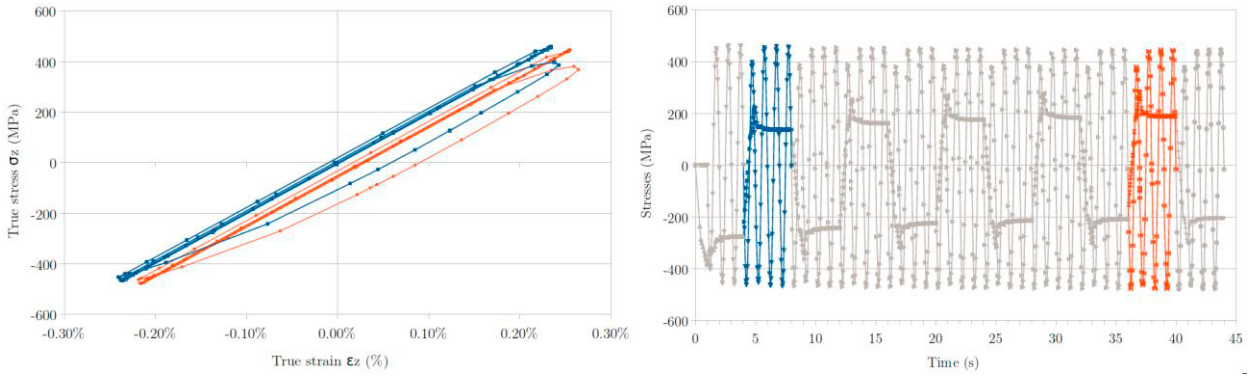

Fig. 7: C3 load case: a) stress strain loops in B; b) time evolution of the stresses at B on 42CrMo4 specimen.

5. Fatigue life calculation methods

5.1. Fatemi-Socie model

The critical plane, P_c, is defined as the maximum shear strain plane [9] [10]. In this plane, the damage parameter, d, is given by the following equation:

$$d = \gamma_{a,max}\left(1 + k\frac{\sigma_{n,max}}{\sigma_y}\right) = (1+\nu_e)\frac{\sigma_f{}'}{E}(2N_f)^b + \frac{k}{2}(1+\nu_e)\frac{\sigma_f{}'^2}{E\sigma_y}(2N_f)^{2b} + (1+\nu_p)\epsilon_f{}'(2N_f)^c + \frac{k}{2}(1+\nu_p)\frac{\epsilon_f{}'\sigma_f{}'}{\sigma_y}(2N_f)^{b+c} \quad (3)$$

The empirical constant k is usually determined by fitting axial and torsional fatigue data [9]. Some parameters of this method have not been identified for calculation of k, therefore G, τ_f', γ_f', b_0 and c_0 were approximated using the following formulas:

$$G = \frac{E}{2(1+\nu_e)}, \tau_f' = \frac{\sigma_f{}'}{\sqrt{3}}, \gamma_f' = \sqrt{3}\epsilon_f', b_0 = b\ etc_0 = c \quad (4)$$

5.2. Smith-Watson-Topper model

In this model the critical plane, P_c, is defined as the plane experiencing the maximal normal strain $\varepsilon_{n,max}$ [11]. In this plane, the damage parameter, d, is given by:

$$d = \sigma_{n,max}\frac{\Delta\epsilon_n}{2} = \frac{\sigma_f{}'^2}{E}(2N_f)^{2b} + \sigma_f{}'\epsilon_f{}'(2N_f)^{b+c} \quad (5)$$

5.3. Wang-Brown model

For the Wang-Brown model the critical plane, P_c, is defined as the plane supporting the maximum shear strain amplitude [12]. In this plane, the normal strain excursion ε_n* is defined by:

$$\epsilon_n * = max_{t\in T}[\epsilon_n(t)] - min_{t\in T}[\epsilon_n(t)] \quad (6)$$

The damage parameter, *d*, is given by the following expression [Wan93]:

$$d = \frac{\Delta\gamma_{max}}{2} + S\epsilon_n * (1 + \nu_e + (1 - \nu_e)S)\frac{\sigma_f{}'}{E}(2N_f)^b + (1 + \nu_p + (1 - \nu_p)S)\epsilon_f{}'(2N_f)^c \quad (7)$$

The value of the empirical coefficient, *S*, is identified thanks to the purely alternated tension-compression fatigue limit (σ_{-1}) and the purely alternated torsion fatigue limit (τ_{-1}) on smooth specimens ($K_t \approx 1$) [12]. The unknown purely alternated torsion fatigue limit (τ_{-1}) has been estimated for the 30NiCrMo8 thanks to $\tau_{-1} = 0{,}68\sigma_{-1}$ [13].

5.4. Cumulative damage rule

Even if several others cumulative damage methods exist [4], [8], we supposed here that the materials studied follow the Palmgreen-Miner linear cumulative damage hypothesis. The developed algorithms were programmed to identify the critical plane for each loading block. These planes were not necessarily identical from one block to another. The Palmgreen-Miner hypothesis was applied without taking into account the orientation of the critical planes. Thus, the calculated damages have been widely overestimated and thereby our approach is in the end conservative.

6. Results of the fatigue life simulations

6.1. Extrapolation of the torsion cycles

As shown by FEA, torsion cycles appear during the C3 load cases (Figures 6 and 7). However, because of the long time needed for computing the elastic-plastic solution of the finite element model (250 h), the computations were stopped before the full stabilization of the stress-strain state. The stabilized values of the shear stress amplitudes were extrapolated from the FEA results after 44 cycles for 42CrMo4 specimen and 34 cycles for 30NiCrMo8. To do that it is assumed that mean shear stress becomes symmetric.
The comparison of the fatigue lives calculated before and after extrapolating the torsion cycles does not show any significant difference. Consequently, the proposed extrapolation is not mandatory. FEA stopped after 44 and 34 cycles are enough for the assessment of the fatigue lives.

6.2. Fatigue life assessment

According to our simulations and with the chosen simple cumulative damage rule, none of the tested fatigue life calculation methods give good results for all the investigated load cases (Figure 8). The efficiency of the tested methods is very dependent on the material and the load cases. With the Smith-Watson-Topper method the results are closest to the experimental data but no real tendency to safe or unsafe results can be drawn (Fig.8a). For the Fatemi-Socie method, nearly all calculated fatigue lives are in the unsafe domain (Fig. 8b). Simulations done with the Wang-Brown approach lead to fatigue lives far and greater than the experimental data (half of the calculated lives tend to infinity, fig.8c). As stated in the presentation of this method, their authors emphasize that their proposal is for low cycle fatigue and does not take into account the mean stress effect. Consequently, this method should not be used for the studied load cases.

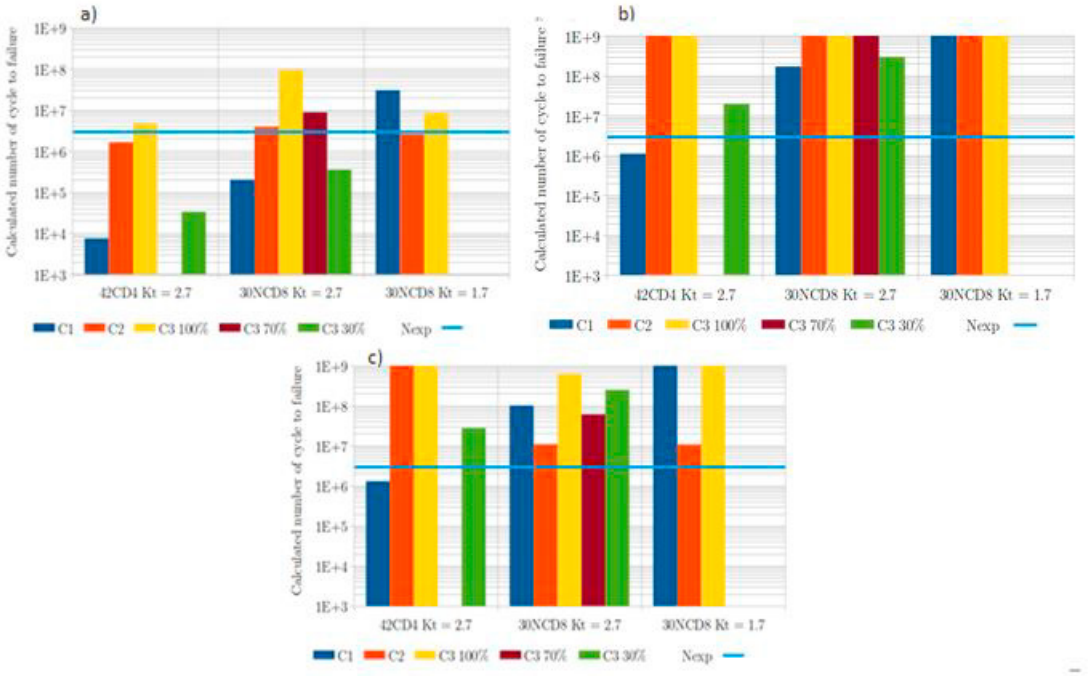

Fig. 8: Fatigue life assessment given by a) Smith-Watson-Topper method; b) Fatemi-Socie method; c) Wang-Brown method

7. Conclusion and prospects

The effect of mean shear stress on the rotative bending (RB) fatigue strength at 3×10^6 cycles was studied on notched specimens (K_t=1.7 and 2.7) made of two quenched and tempered steels. As known in literature, it has been shown that a constant mean shear stress has a negligible influence on the HCF strength under RB for the two grades. But, in intermittent service conditions where repeated cycles of torsion are introduced, it has been shown that these cycles can affect significantly the RB HCF strength at 3×10^6 cycles, depending on the notch acuity and torsion level applied. In the case of K_t = 2.7, for both materials, the rotating bending strength reduction reached 30% for a torsion level equal to the yield strength in shear. This reduction becomes significant only for a mean torsion level over 30% of the yield strength in torsion. Although this effect was not observed in the case of K_t = 1.7, it seems relevant to consider in general that the damage induced by these repeated cycles is not negligible beyond a torsion level of 30% of the yield strength in shear.

An elastic-plastic finite element analysis shows that the stabilized stress-strain field is not axi-symmetric all around the notch root because of plastic strains occurring during the first loading. This creates a non axi-symmetric field of residual stresses. According to our simulations and with the chosen cumulative damage rule (Palmgreen-Miner), none of the tested fatigue life calculation methods give good results for all the load cases. The efficiency of the tested methods is very dependent on both the material and the load cases. However, the Smith-Watson-Topper approach gives the best results whereas the Fatemi-Socie or Wang Brown models lead to the more non conservative ones except in one load case.

References

[1] DIN 743-1, Calculation of load capacity of shafts and axles - Part 1: General, German Standard, 2012.
[2] NFE 22 057-1, Mechanical Transmissions - Shafts and Axles, Calculation of load capacity - Part 1: General, AFNOR, 2012.
[3] T. Palin-Luc, S. Lasserre, A multiaxial fatigue testing machine for variable amplitude loadings of bending and torsion, In Proc. 4th ICBMFF, Vol. 1, May 31 - June 3, 1994, Paris, pp. 449-459.
[4] J. Lemaitre, J.L. Chaboche, A. Benallal and al, Mécanique des matériaux solides-3eme édition, Dunod, 2009.
[5] T. Palin-Luc, N. Saintier, J.L Charles, Calculs élastoplastiques en fatigue à l'aide du critère énergétique et volumique de fatigue multiaxiale du LAMEFIP, Rapport interne LAMEFIP, 2006.
[6] J.F. Flavenot, C. Lecointe, Courbe unique de comportement en fatigue, rapport interne CETIM, 2007.
[7] M. Bennebach, Fatigue multiaxiale d'une fonte GS. Influence de l'entaille et d'un traitement de surface, PhD thesis, ENSAM, 1993.
[8] A. Banvillet, Prévision de durée de vie en fatigue multiaxiale sous chargements réels : vers des essais accélérés, PhD thesis, ENSAM, 2001.
[9] A. Fatemi, D.F. Socie, A critical plane approach to multiaxial fatigue damage including out-of -phase loading, Fatigue & Fracture of Engineering Materials & Structures, 1988, vol. 11, no 3, p. 149-165.
[10] N. Shamsaei, A. Fatemi, Effect of hardness on multiaxial fatigue behaviour and some simple approximations for steels, Fatigue & Fracture of Engineering Materials & Structures, 2009, vol. 32, no 8, p. 631-646.
[11] J.A. Bannantine, D.F Socie, A variable amplitude multiaxial fatigue life prediction method, In : ICBMFF3, 2013, ESIS
[12] CH. Wang, MW. Brown, A path-independent parameter for fatigue under proportional and non-proportional loading, Fatigue & Fracture of Engineering Materials & Structures, 1993 Dec 1;16(12):1285-97.
[13] A. Brand and al, Recueil de données technologiques sur la fatigue, CETIM, 1980.